PAPER

Check for updates

Sulfonation of alginate grafted with polyacrylamide as a potential binder for high-capacity Si/C anodes†

Bolormaa Gendensuren,‡ Chengxiang He‡ and Eun-Suok Oh [ID] *

A systematic approach for how to find an appropriate polymer binder for high-capacity LIB anodes is presented in this study. As an example, a newly-developed SAlg-*g*-PAAm binder, alginate functionalized with sulfo groups and subsequently grafted with polyacrylamide, is used for the Si/C electrode. Various characteristics of the binder polymer itself, two basic characteristics of the electrode with respect to the binder, and the effect of the binder on cell performance are subsequently investigated. In all respects, the SAlg-*g*-PAAm polymer is a very promising binder for high-capacity anodes. The sulfo groups in the binder improve the ionic conductivities in both the binder and the electrode, leading to reduced charge transfer resistance. In addition, the sulfonation of the alginate grafted with polyacrylamide significantly enhances the mechanical and adhesion properties of the binder and consequently decreases the volume change generated during cycles. These advantages of the SAlg-*g*-PAAm binder ultimately lead to a considerable enhancement in the electrochemical performance of the high-capacity Si/C electrodes.

Introduction

Polymeric binder is a crucial component of ensuring electrical integrity due to its cohesion and adhesion capability in lithium-ion battery (LIB) electrodes. An efficient binder can buffer the volume change caused by the insertion/de-insertion of lithium ions in the course of operation, resulting in enhanced battery performance.[1,2] A number of recent papers have demonstrated the importance of selecting an appropriate polymer binder for high capacity anodes experiencing huge volume changes, such as silicon and their composites.[3–6] Polysaccharide binders such as carboxymethyl cellulose (CMC),[7,8] sodium alginate (Alg),[9] and other modified polysaccharides including copolymerizations and blends[10–13] have shown excellent binder performance for silicon-based anodes compared to commercial polyvinylidene fluoride (PVDF) binder. However, their insulating nature in electronic and ionic conduction still impedes the high-power performance of the electrodes, although some progress was achieved by modifying the polysaccharide matrices through blending and grafting them with electroactive oligomers or small molecular groups.[14–17]

The blending of polysaccharide-based binders with a polymer containing ionically conductive groups provides a substantial enhancement of lithium ion transport in the electrode, and thus improves the cycling behavior of Si-based

School of Chemical Engineering, University of Ulsan, 93 Daehak-ro, Nam-Gu, Ulsan 44610, Republic of Korea. E-mail: esoh1@ulsan.ac.kr; Fax: +82-52-259-1689; Tel: +82-52-259-2783

† Electronic supplementary information (ESI) available. See DOI: 10.1039/d0ra07557d

‡ Equally contributed to this work.

anodes. Recent works have demonstrated that the lithium ion conduction in polymeric binder is significantly improved with the addition of polyethylene glycol (PEG) to polysaccharide and other polymeric binders, leading to enhanced electrochemical performance of Si-based anodes.[17,18] Lee *et al.*[18] reported that blending and crosslinking between CMC and PEG led to stable cycling performance with a capacity of almost 2000 mA h g^{-1} up to 350 cycles due to the strong adhesion ability stemming from the CMC blocks as well as the facile lithium ion movement originating from the PEG *block*. PEG-based *block* or *graft* copolymers have also been examined as high performance binders for Si anodes.[15,16,19] For example, triblock linear copolymer polydopamine–polyacrylic–polyoxyethylene binder has been shown to improve the cycle performance and reversible capacity for silicon anodes compared to Si/PVDF electrode due to its strong adhesion and high ion conductivity.[15]

Some studies on grafting high adhesive polymer to polysaccharide binder have also shown enhanced electrochemical performance of Si anodes.[20,21] Polysaccharides grafted with polyacrylic acid (PAA) have shown excellent binder properties for Si anodes compared to traditional linear polysaccharides due to the high binding ability of branched PAA to Si active materials.[6,12] Recently, we showed that using alginate grafted with polyacrylamide (PAAm) improved the electrochemical performance of Si-based electrodes; this was attributed to the high adhesion of the PAAm *block*.[22] Although the grafted binder gives better adhesion to the active material and the current collector, it is still necessary to enhance the ionic conductivity for high-powered electrodes.

The molecular designs of sulfonated polymers have mostly been simulated for an ionic liquid membrane of fuel cells and

LIBs due to the high ionic conductivity of the sulfonated chain in the polymer.[23–25] A few studies have proposed sulfonated aromatic polymers, such as sulfonated poly(ether-ether-ketone) (SPEEK) and sulfonated polystyrene, as ionic conductivity binders for sulfur cathodes of Li–S batteries and LiFePO$_4$ cathodes of LIB.[26–28] They reported that, compared to the conventional PVDF binder, the sulfonic aromatic chain in the binder led to better electrochemical performance of the cathodes. Qin et al.[29] also developed a SPEEK–PSI–Li binder containing lithiated fluorinated sulfonimide groups for high-capacity Si electrodes. The Si/SPEEK–PSI–Li electrode maintained a specific capacity over 500 mA h g^{-1} at a high current rate, whereas the electrodes composed of PVDF, CMC, and Alg had nearly a zero capacity at that same current rate. This high capacity was attributed to the improved lithium ion transport of sulfonate groups in the binder. However, the SPEEK-based copolymer binders still require a non-ecofriendly 1-methyl-2-pyrrolidone organic solvent for the dissolving process.

Recently, our group developed a one-step process for preparing sulfonated polysaccharides in eco-friendly water solvent, and successfully applied this process to the development of a high-powered Li$_4$Ti$_5$O$_{12}$ anode.[30] In this study, we extend our studies to further improve the binder performance. The Alg polymer is first sulfonated for lithium ionic conduction, then the sulfonated Alg is grafted with adhesive PAAm through the polymerization of AAm monomer, and the sulfonated and grafted binder is applied to a high-capacity silicon/graphite (Si/C) anode as an inactive binder material. Finally, various characterization tools are used to systematically analyze the character of the developed binder.

Experimental

Preparation of sulfonated alginate backbone

To prepare sulfonated Alg (denoted by SAlg), a 2.8 g of sodium Alg (Alfa Aesar Co. Ltd) was dissolved in 100 ml of phosphate buffer solution (PBS, pH ∼ 6.0) under harsh stirring at room temperature. 4.8 g of N-ethyl-N′-(3-dimethylaminopropyl) carbodiimide hydrochloride and 1.09 g N-hydroxysuccinimide dissolved in the buffer solution were added into the Alg-PBS solution under stirring to activate the carboxylic groups in Alg. After 15 min, 3-amino-1-propanesulfonic acid was added to the solution, and trimethylamine was also added dropwise to achieve pH ∼ 7.4. The reaction was maintained for 9 h under continuous stirring at room temperature. The reaction products collected by suction filtration were washed with water and then ethanol before being dried in a vacuum oven at 50 °C.

Synthesis of sulfonated alginate grafted with polyacrylamide

In situ free radical polymerization was used to produce PAAm grafted onto polysaccharide (natural Alg and SAlg) backbones in water medium with ammonium persulfate (APS) as a radical initiator and tetramethyl-ethylenediamine (TEMED) as a reaction accelerator. All chemicals used in this study were purchased from Sigma-Aldrich Co. Ltd, and the total

Table 1 Ingredients of the *graft* copolymerization (g)

Sample	Alg	SAlg	AAm	APS	TEMED
Alg-g-PAAm	2.8	0.0	10	0.06	0.055
SAlg-g-PAAm	0.0	2.8	10	0.06	0.055

composition is listed in Table 1. The grafting procedure was described in detail in our previous study.[22]

Preparation of electrodes and cells

To prepare the working electrodes, silicon/graphite with a weight ratio of 1/3 and super-P (SP) conductive carbon black were mixed with polymeric binder based on the respective weight ratio of 76 : 9 : 15 in water. The well-mixed slurry was then cast onto copper foil using the doctor-blade method, dried in a convection oven at 70 °C for 30 min, and dried again in a vacuum oven at 70 °C overnight before being assembled in a cell. The mass loadings of the Si/C electrodes were 1.1 ± 0.1 mg cm^{-2}. CR2032 coin-half cells were assembled in an argon-filled glove-box using the Si/C working electrode, Li foil as a counter and reference electrode, 1.15 M LiPF$_6$ ethylene carbonate/diethyl carbonate/dimethyl carbonate (3/5/2 vol%) with additives (5 wt% fluoroethyl carbonate, 2 wt% vinylene carbonate and 0.4 wt% LiBF$_4$) as the electrolyte (Enchem Co. Ltd), and a polypropylene separator (Celgard LLC).

Physical characterization of polymer binders

The Alg-based polymers were analyzed by Fourier-transform infrared (FT-IR, Thermo Scientific Nicolet iS5) spectroscopy as well as thermogravimetric analysis (TGA, Q50, TA Instruments) under nitrogen atmosphere using aluminum pans with a heating rate of 10 °C. The binder films were elongated using a texture analyzer (TA-PLUS, Lloyd Instruments Ltd). For the preparation of the sample for the elongation test, grafted copolymer was first dissolved in distilled water containing 30 wt% glycerol to polymer as a plasticizer. The ionic conductivity of the membrane was measured at the potential of OCV. The amplitude in the voltage was 7 mV and the frequency ranged from 1 Hz to 10^6 Hz. The membranes were assembled into two pairs of the stainless-steel electrode in coin-cell 2032 with carbonate electrolyte. The ionic conductivity was calculated using

$$\sigma = \frac{L}{AR} \qquad (1)$$

where σ is the ionic conductivity, L is the thickness of the membrane, R is the resistance of the membrane, and A is the surface area.

Physical and electrochemical characterizations of the Si/C electrode

The adhesion strength of the Si/C electrodes was obtained using the same procedures described in our previous study.[22] The sheet resistances of the electrodes were measured using a four-

point probe system (CMT-100 MP, Advanced Instrument Technology). The surface morphologies of the fresh and cycled Si/C electrodes were characterized by plain-view field-emission scanning electron microscopy (FE-SEM Jeol, JSM-6500F). The galvanostatic charge/discharge of the coin-half cell was measured between 5 mV and 1.5 V at a current rate of 0.1C for the first two cycles and at a current rate of 0.5C for the subsequent 200 cycles, whereas the rate capability was controlled at various current rates ranging from 0.1C to 10C. Cyclic voltammetry (CV) was performed at the scan rate of 0.2 mV s^{-1} within potentials ranging from 5 mV to 3 V $vs.$ Li$^+$/Li. Electrochemical impedance spectroscopy (EIS) was performed at 0.2 V $vs.$ Li$^+$/Li under a frequency range of 0.01 Hz to 100 kHz and an amplitude voltage of 7 mV. EIS and CV were respectively carried out using HS-2E and HS-3E TK flat cells (HOSEN Corp./Japan) on a BioLogic Science Instrument. The change in the thickness of electrodes was examined using an in $situ$ electrochemical dilatometer (ECD-3, El-Cell GmBH), and the experiment processor was explained in our previous study.[22]
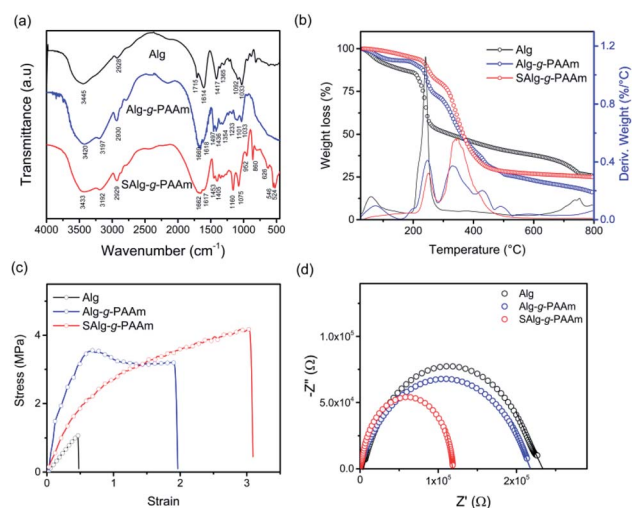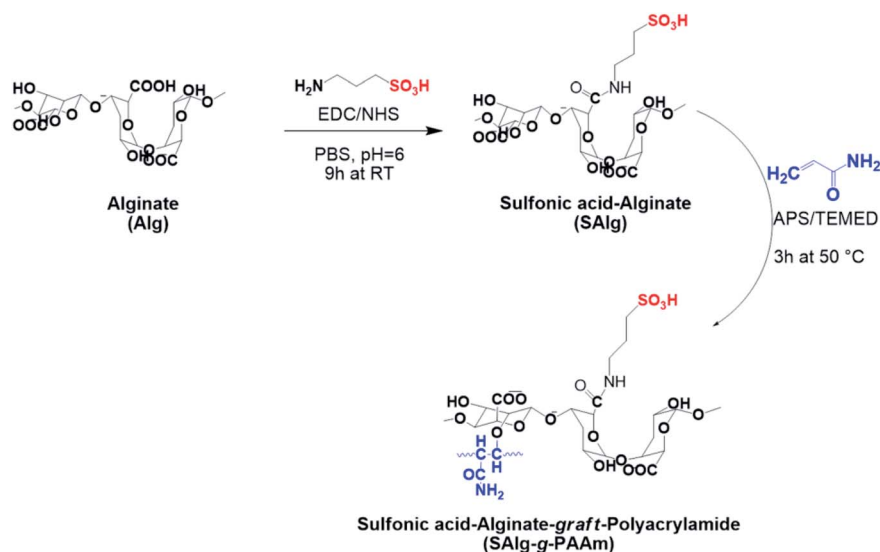

Fig. 1 (a) FT-IR spectra, (b) TGA profiles, (c) stress−strain curves, and (d) Nyquist plots of natural Alg and modified Algs through functionalization with sulfo group and grafting with PAAm.

Results and discussion

The two-step synthetic procedure of sulfonated alginate-$graft$-polyacrylamide (SAlg-g-PAAm) is illustrated in Scheme 1. The Alg was first sulfonated and then grafted with PAAm through the polymerization of AAm on the SAlg backbone.

The FT-IR spectra of natural and modified Algs are shown in Fig. 1a. Compared to the FT-IR spectrum of natural Alg, two strong characteristic peaks observed at 1092 and 1033 cm^{-1} corresponding to CH–OH bending vibration and C–O–C stretching, respectively, are weakened in the modified Alg copolymers, the Alg-g-PAAm and SAlg-g-PAAm samples, which is attributable to the formation of chemical bonds between hydroxyl groups in Alg and p bands in PAAm.[22,31] In addition, four new adsorption peaks near 3195 cm^{-1}, 1665 cm^{-1}, 1617 cm^{-1}, and 1436 cm^{-1}, respectively assigned to the

stretching of NH$_2$, CO–NH$_2$, and C–N of the PAAm chain (Fig. S1†), can be seen in the spectra of the grafted samples. Compared to the unsulfonated Alg-g-PAAm, the FT-IR spectrum of SAlg-g-PAAm shows two new strong peaks at 1075 and 1160 cm^{-1}, which are respectively attributed to the presences of –SO$_3^-$ symmetric stretching and S–O–H bending.[32–34] The S–O and C–S stretching bands were also observed at the ranges of 952 and 700–500 cm^{-1}, respectively, on the FT-IR spectrum of SAlg-g-PAAm (Fig. 1a).

The thermal stability of the binder was characterized using TGA, and the result is illustrated in Fig. 1b. Excluding the initial weight loss under 200 °C, which is related to the evaporation of absorbed water, the natural Alg exhibits substantial weight loss around 250 °C, which is attributed to the loss of CO$_2$ of

Scheme 1 Synthesis of sulfonated SAlg-g-PAAm: sulfonation of Alg backbone and grafting of the sulfonated Alg with PAAm.

polysaccharide chains.[31] This decomposition was slightly retarded in the grafted Alg samples, Alg-g-PAAm and SAlg-g-PAAm. Both of the grafted Algs showed degradation above 300 °C, which corresponds to the loss of NH_2 in PAAm Fig. 1b.[31] Similar to the result reported by Biswal and Singh,[31] the grafting of PAAm to Alg improves the thermal stability of Alg. Moreover, it is clear that the sulfonation makes the grafted Alg-g-PAAm more thermally stable.

Next, the mechanical properties of the natural and modified Alg films containing glycerol plasticizers were measured through tensile strength tests. As shown in Fig. 1c, the Alg backbone grafted with PAAm was found to have a much higher stress and strain at break than natural Alg. Our target sample, the sulfonated and grafted SAlg-g-PAAm, exhibited further increases in both the stress up to 4.5 MPa and the strain up to 3.2 at break. These are attributed to the formation of strong cohesion between polymer chains by the sulfonate ionic groups.[32,35,36] Such a large increase in binder elongation is expected to be more useful for electrodes, particularly for high capacity anodes that experience significant volume expansion during the charge/discharge processes, such as Si or Sn.[37] As a final physical characteristic of the bare polymers, the ionic conductivities of the polymer films placed between two parallel stainless-steel electrodes were determined through EIS testing. The measurement process was described in further detail by Chauque et al.[38] The electrical resistance of the film can be estimated from the x intercept of the Nyquist plot (Fig. 1d). As a result, the ionic conductivities of the dry membranes are 2.98×10^{-8} S cm^{-1} for Alg, 3.21×10^{-8} S cm^{-1} for Alg-g-PAAm, and 5.68×10^{-8} S cm^{-1} for SAlg-g-PAAm. The improvement in the ionic conductivity was also confirmed by the result regarding the ionic conductivity of the binder solution. The aqueous SAlg-g-PAAm solution has higher ionic conductivities regardless of the presence of electrolyte when compared to the aqueous Alg-g-PAAm solution (Fig. S2†). These results are consistent with previous ones reported by Rohan et al.[32] and Pang et al.[39] They proposed that the strong electron withdrawing capability of sulfo-like groups increases the ionic conductivity of the polymer membranes functionalized by the sulfo groups. Therefore, enhancing the sulfonation of the polymer binder is an efficient way to improve its ionic conductivity, and may also help lithium ion transport in the Si/C electrodes.

Additionally, CV of the binder composite mixed physically with 50 wt% SP carbon black was conducted in the range of 0–3.0 V vs. Li$^+$/Li to examine its electrochemical stability as an anodic binder. As shown in Fig. S3,† no faradaic peaks related to the polymers appear in the profiles, except for the peaks assigned to the lithiation of SP,[40] indicating that all the binders are electrochemically stable in the anodic working voltage; even the redox peaks disappear in the SAlg-g-PAAm sample. This may contribute to the better dispersion of SP and subsequent reduced formation of SP clusters in the sulfonated polymer for current flow relative to the other two polymers.

Summarizing the above results, it can clearly be seen that the sulfonation of the binder polymer is favorable in all respects: thermal, mechanical, and electrochemical stabilities, and ionic conduction. When a new polymer is first applied to a binder for electrodes, the adhesion strength and the electrical resistance of the electrodes should be examined before testing the electrochemical performance of the polymer within electrodes. These are basic properties mainly originating from the binder that can be used to roughly predict the electrode performance in advance. The results of the two experiments are distinguished in Fig. 2 according to the binder materials. Compared to natural Alg, the presence of the multipoint functional groups in the branched structure of the Alg-g-PAAm binder significantly increases the electrode adhesion from ~2 N up to ~10 N.[22] Even further functionalization by the sulfonation in the binder increases the adhesion by 50%, as shown in Fig. 2a. By contrast, as shown in Fig. 2b, the electrical resistances of the electrodes are not as susceptible to the binder materials due to the fact that there is little change in their electrical insulating nature, even though the SAlg-g-PAAm-containing electrode has slightly less resistance than the other two electrodes.

Rather, the difference might be explained by means of the possibility of the improved dispersion of SP in the electrode containing the SAlg-g-PAAm binder. For the high-capacity anodes composed of Si, strong electrode adhesion is favorable because they have to overcome the high stress caused by the substantial volumetric change that occurs during the charge/discharge processes. Consistent with the results of the binder itself shown in Fig. 1, S2 and S3,† the sulfonation of the binder therefore also gives rise to positive effects on the Si/C electrodes.
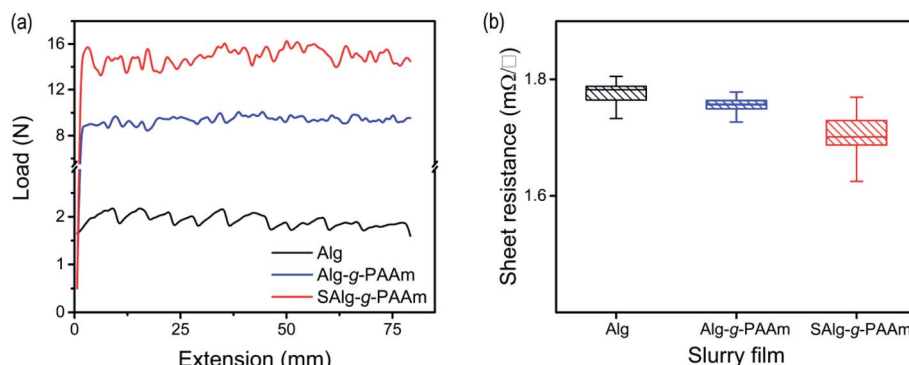

Fig. 2 (a) Adhesion strength of the Si/C electrodes containing different binders measured by 180° peel test and (b) sheet resistances of 25 μm thick Si/C slurry films.

Finally, the electrochemical performances of the Si/C electrodes containing different binders were measured using CV, EIS, galvanostatic cycling, and *in situ* ECD techniques, and the results are shown in Fig. 3. Excluding the peaks around 1.0 V *vs.* Li⁺/Li, which correspond to the formation of SEI at the first cycles shown in Fig. 3a, the CV profiles of the Si/C electrodes exhibit two cathodic peaks near 4.8 mV and 0.23 V for lithiation and two corresponding anodic peaks near 0.28 V and 0.47 V for delithiation. It should be noted that the intensity and the area of the redox peaks, as well as the potential difference in the redox peaks, are clearly distinguished according to the binder used for the Si/C electrodes. The peak area is related to the amount of charge flow during the scanning, whereas the potential difference informs the relative polarization resistance for the electrochemical redox reaction. The electrode containing the SAlg-*g*-PAAm has a substantially broader peak area with a higher intensity and a lower potential difference in the redox peaks than those containing the other two binders, natural Alg and unsulfonated Alg-*g*-PAAm. This means that the sulfonated binder contributes to better lithium ion transport in the electrode, as was already proven in Fig. 1d and S2,† and this is mainly attributed to the negative sulfonate ions in the binder. This improvement was also confirmed by the EISs of the coin-half cells composed of the Si/C working electrodes (Fig. 3b). The cells were cycled twice at 0.1C, twice at 0.2C, and twice at 0.5C, respectively, before being measured by EIS at 0.2 V. Although multiple interpretations exist of Nyquist plots of LIBs, it is generally accepted that LIBs are modelled with the equivalent electrical circuit shown in Fig. S4d.† R_s at the very high frequency is related to the ohmic resistance of the bulk electrolyte, whereas the RQ parallel circuit, as represented by a semicircle at the high frequency region in the Nyquist plot, models the contact problem between the current collector and the electrode layer, as well as between active materials in the electrode layer, and the lithium ion migration through SEI film.

The final RQ combined with the Warburg diffusion element is closely related to the charge transfer resistance and solid-state diffusion of lithium ions in the material, and this is represented by the semicircle at the middle frequency range with the 45° linear line at a very low frequency.[41,42] It can clearly be seen in Fig. 3b that the sulfonation in the binder is a modification that substantially decreases the resistances caused by physical contact, SEI formation, and charge transfer reactions. More precisely, as shown in Fig. S4,† the grafting of Alg with PAAm could prevent the increase in the resistances of the Alg-containing Si/C electrode, and the sulfonation of the grafted Alg-*g*-PAAm could further diminish the resistances. This must originate from the superior ionic conduction and adhesion of the SAlg-*g*-PAAm binder. In general, the resistances decrease with repeated charge/discharge cycles because adjustments to the internal components occur, such as the infiltration of the electrolyte in the electrode and the compact relation in the electrode structure, which facilitate the movements of lithium ions and electrons.[43,44] By contrast, the resistances possibly increase if the electrolyte dries up due to irreversible electrolyte decomposition, or if damage (or looseness) occurs to the electrode structure in the course of cycling. Therefore, the increase in the resistance of the Alg-containing Si/C electrode with cycling is mainly due to the occurrence of more severe damage in the electrode originating from the low electrode adhesion, as shown in Fig. 2a, when compared to the other electrodes. This will also be proven in the experiments on the cyclic performance, volumetric expansion, and morphology of the electrodes.

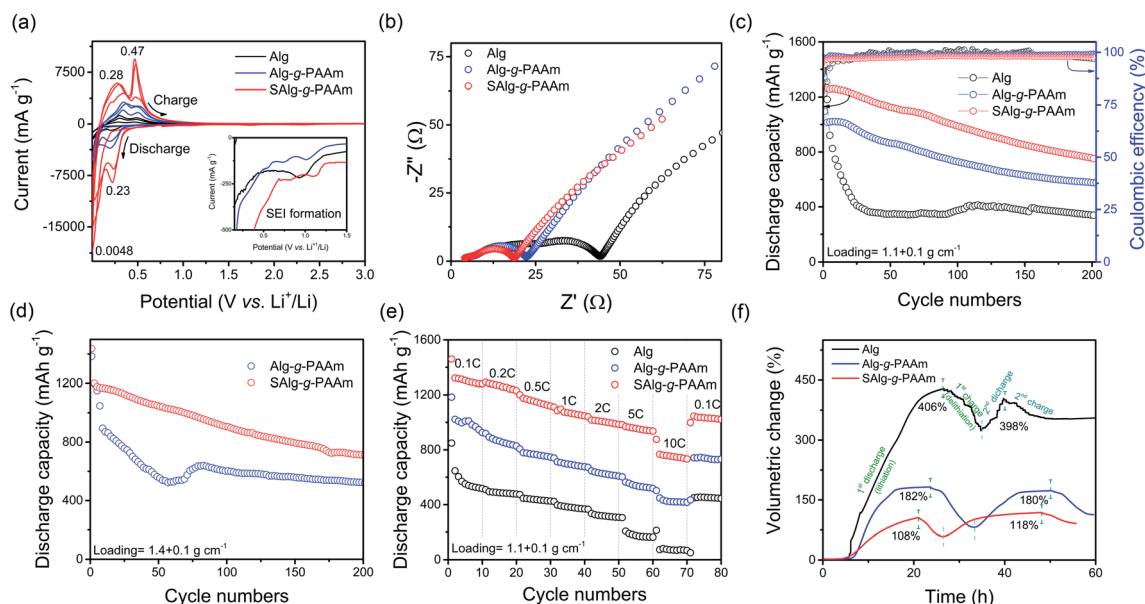The cyclic performances of the Si/C electrodes with two different mass loadings are displayed in Fig. 3c and d.

Fig. 3 (a) Cyclic voltammogram of the Si/C electrodes containing different binders, (b) Nyquist plots of the cycled Si/C electrodes at the DC potential of 0.2 V, (c) and (d) cyclic performances of the Si/C electrodes with difference mass loadings, (e) rate capability test results of the Si/C electrodes, and (f) volumetric change of the Si/C electrodes over the course of two charge/discharge cycles at 0.1C.

Regardless of the binder materials and the loadings, a notable decrease in capacity is observed in the first few cycles. However, the extent of the decrease is distinguishable according to the binder materials. The Si/C electrodes using low adhesive binders, such as natural Alg in particular, experience severe capacity fading for quite long cycles before stabilization, due to the presence of graphite, whereas the electrode using the SAlg-g-PAAm binder shows a relatively gentle decrease and remains at the specific capacity of 750 mA h g^{-1}, even up to 200 cycles. By contrast, the Alg-g-PAAm- and Alg-containing electrodes are 651 and 381 mA h g^{-1}, respectively. Similar results were observed for the Si/C with a higher loading of 1.4 ± 0.1 mg cm^{-2}. As shown in Table S1 of the ESI,† this result is considerably superior to previous studies, even though the electrochemical performance of the Si/C electrodes is also dependent upon electrode formulation, electrode mass loading, cycling condition, and so on. Furthermore, the results of the rate capability tests ranging from 0.1C to 10C presented in Fig. 3e clearly show the advantage of using the sulfonated SAlg-g-PAAm binder in the high-capacity Si/C electrode. At the highest current, the SAlg-g-PAAm electrode remains at a capacity of more than 700 mA h g^{-1}, while the unsulfonated Alg-g-PAAm and natural Alg electrodes have less than 500 and 100 mA h g^{-1}, respectively.

The *in situ* electrochemical dilatometer technique[22,45,46] was used to track the change in the volume (more specifically, the thickness) of the Si/C electrode during the charge/discharge process, and the results are illustrated in Fig. 3f; it can be seen in the figure that the volume change is greatly dependent upon the binder used for the electrode. The sulfonated binder-containing electrode experiences only a 108% increase during the first discharge (lithiation) process, which is close to its theoretical value of 65%. Based on the electrode composition of 76 : 9 : 15 Si/C : SP : binder, the theoretical value was calculated from theoretical increases of 310% for Si, 10% for graphite, and zero for SP and binder. By contrast, the Si/C electrodes containing unsulfonated Alg-g-PAAm and natural Alg are 182% and 406%, respectively, which are significantly larger than the theoretical value. In the subsequent charge (delithiation) process, the electrode swelling is somewhat alleviated in all three electrodes, but large residual swelling still remains after the first cycle. Even the Alg-electrode exhibits 340% after the second cycle, whereas the grafted binders show substantially less residual swelling: 113% for the Alg-g-PAAm electrode and 91% for the SAlg-g-PAAm electrode. Such high electrode swelling might cause severe damage in the electrode network, ultimately leading to notable capacity fading for the first few cycles, as shown in Fig. 3c.

Clear evidence for the damage in the electrode can be seen in Fig. 4, which presents SEM images of the fresh and 200-cycled electrodes. The cycled electrodes were obtained by disassembling the coin cell cycled 200 times at 0.5C in an argon-filled glove box. Compared to the fresh electrodes, the cycled electrodes show a crushable and porous structure on their surfaces due to the huge volumetric change of Si and the formation of SEI layer on the Si surface. More importantly, cracks occur in the electrodes in both the Alg and the Alg-g-PAAm electrodes, whereas the SAlg-g-PAAm electrode withstands the volume
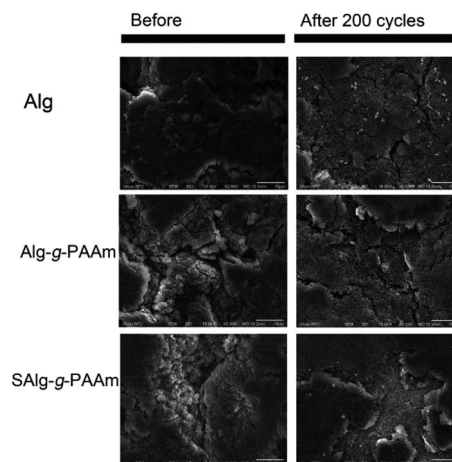

Fig. 4 Top-view SEM analyses of the Si/C fresh and 200-cycled electrodes.

increase shown in Fig. 3f and thus forms fewer cracks than the other two electrodes.

In conclusion, the sulfonation of the grafted Alg-g-PAAm binder forms stronger adhesion and larger elongation in the electrode and thus prevents huge volumetric expansion and mechanical cracks during cycling. These advantages, combined with the enhancement of lithium ion transport in the electrode, consequently contribute to the electrochemical improvements in the Si/C electrodes shown in Fig. 3c–e that are achieved by the use of sulfonated and grafted SAlg-g-PAAm binder.

Conclusions

The SAlg-g-PAAm binder consisting of alginate functionalized with the sulfo groups and subsequently grafted with polyacrylamide is used as an example of a systematically researched binder for the high-capacity Si/C electrode. First, the thermal and electrochemical stabilities of the binder polymer itself are examined, along with its mechanical and electrical properties (ionic conduction). The sulfonation of the binder polymer is favorable in all respects. Next, two basic properties of the electrode that mainly originate from the binder are necessarily examined to obtain a rough prediction of the electrode performance: the adhesion strength and the electrical resistance of the electrode. The multipoint functional groups in SAlg-g-PAAm that occur with the sulfonation and the grafting with PAAm increase the adhesion by four times compared to natural Alg, although little change occurs in the electrode resistance due to the instinct-insulating nature of the polymer binders. Finally, the effects of the binder on the electrochemical performances of the Si/C electrodes are thoroughly investigated through CV, EIS, galvanostatic cycling, and *in situ* ECD techniques. Due to the ion conduction, high adhesion, and good mechanical characteristics of the SAlg-g-PAAm binder, the Si/C electrode has low polarization (or charge transfer) resistance and a small volume change, and thus suffers less damage during repeated cycles, all of which ultimately lead to substantially better cyclic

performance when compared to parent and unsulfonated grafted Alg binders, even at high current rates.

Conflicts of interest

There are no conflicts to declare.

Acknowledgements

References

1 S.-L. Chou, Y. Pan, J.-Z. Wang, H.-K. Liu and S.-X. Dou, *Phys. Chem. Chem. Phys.*, 2014, **16**, 20347–20359.

2 M. H. T. Nguyen and E.-S. Oh, *J. Electroanal. Chem.*, 2015, **739**, 111–114.

3 N. Ding, J. Xu, Y. Yao, G. Wegner, I. Lieberwirth and C. Chen, *J. Power Sources*, 2009, **192**, 644–651.

4 H. Wu and Y. Cui, *Nano Today*, 2012, **7**, 414–429.

5 D. Bresser, D. Buchholz, A. Moretti, A. Varzi and S. Passerini, *Energy Environ. Sci.*, 2018, **11**, 3096–3127.

6 P.-F. Cao, M. Naguib, Z. Du, E. Stacy, B. Li, T. Hong, K. Xing, D. N. Voylov, J. Li, D. L. Wood, A. P. Sokolov, J. Nanda and T. Saito, *ACS Appl. Mater. Interfaces*, 2018, **10**, 3470–3478.

7 H. Buqa, M. Holzapfel, F. Krumeich, C. Veit and P. Novák, *J. Power Sources*, 2006, **161**, 617–622.

8 J. Li, R. B. Lewis and J. R. Dahn, *Electrochem. Solid-State Lett.*, 2007, **10**, A17–A20.

9 I. Kovalenko, B. Zdyrko, A. Magasinski, B. Hertzberg, Z. Milicev, R. Burtovyy, I. Luzinov and G. Yushin, *Science*, 2011, **334**, 75–79.

10 B. Koo, H. Kim, Y. Cho, K. T. Lee, N.-S. Choi and J. Cho, *Angew. Chem., Int. Ed.*, 2012, **51**, 8762–8767.

11 L. Chai, Q. Qu, L. Zhang, M. Shen, L. Zhang and H. Zheng, *Electrochim. Acta*, 2013, **105**, 378–383.

12 L. Wei, C. Chen, Z. Hou and H. Wei, *Sci. Rep.*, 2016, **6**, 19583.

13 D. V. Carvalho, N. Loeffler, M. Hekmatfar, A. Moretti, G.-T. Kim and S. Passerini, *Electrochim. Acta*, 2018, **265**, 89–97.

14 V. L. Finkenstadt, *Appl. Microbiol. Biotechnol.*, 2005, **67**, 735–745.

15 L. Lü, H. Lou, Y. Xiao, G. Zhang, C. Wang and Y. Deng, *RSC Adv.*, 2018, **8**, 4604–4609.

16 W. Zeng, L. Wang, X. Peng, T. Liu, Y. Jiang, F. Qin, L. Hu, P. K. Chu, K. Huo and Y. Zhou, *Adv. Energy Mater.*, 2018, **8**, 1702314.

17 M. Ling, J. Qiu, S. Li, C. Yan, M. J. Kiefel, G. Liu and S. Zhang, *Nano Lett.*, 2015, **15**, 4440–4447.

18 D. Lee, H. Park, A. Goliaszewski, Y. Byeun, T. Song and U. Paik, *Ind. Eng. Chem. Res.*, 2019, **58**, 8123–8130.

19 C.-H. Tsao, C.-H. Hsu and P.-L. Kuo, *Electrochim. Acta*, 2016, **196**, 41–47.

20 L. Wei and Z. Hou, *J. Mater. Chem. A*, 2017, **5**, 22156–22162.

21 Y. Gao, X. Qiu, X. Wang, A. Gu, L. Zhang, X. Chen, J. Li and Z. Yu, *ACS Sustainable Chem. Eng.*, 2019, **7**, 16274–16283.

22 B. Gendensuren and E.-S. Oh, *J. Power Sources*, 2018, **384**, 379–386.

23 R. Zhou, W. Liu, Y. W. Leong, J. Xu and X. Lu, *ACS Appl. Mater. Interfaces*, 2015, **7**, 16548–16557.

24 Y. Liu, Z. Cai, L. Tan and L. Li, *Energy Environ. Sci.*, 2012, **5**, 9007–9013.

25 L. Zanchet, L. G. da Trindade, W. Bariviera, K. M. Nobre Borba, R. D. M. Santos, V. A. Paganin, C. P. de Oliveira, E. A. Ticianelli, E. M. A. Martini and M. O. de Souza, *J. Mater. Sci.*, 2020, **55**, 6928–6941.

26 Z. Wei, L. Xue, F. Nie, J. Sheng, Q. Shi and X. Zhao, *J. Power Sources*, 2014, **256**, 28–31.

27 M. Cheng, L. Li, Y. Chen, X. Guo and B. Zhong, *RSC Adv.*, 2016, **6**, 77937–77943.

28 M. Cheng, Y. Liu, X. Guo, Z. Wu, Y. Chen, J. Li, L. Li and B. Zhong, *Ionics*, 2017, **23**, 2251–2258.

29 D. Qin, L. Xue, B. Du, J. Wang, F. Nie and L. Wen, *J. Mater. Chem. A*, 2015, **3**, 10928–10934.

30 C. He, B. Gendensuren, H. Kim, H. Lee and E.-S. Oh, *J. Electroanal. Chem.*, 2020, 114532.

31 D. R. Biswal and R. P. Singh, *Carbohydr. Polym.*, 2004, **57**, 379–387.

32 R. Rohan, Y. Sun, W. Cai, Y. Zhang, K. Pareek, G. Xu and H. Cheng, *Solid State Ionics*, 2014, **268**, 294–299.

33 F. Wang, M. Hickner, Y. S. Kim, T. A. Zawodzinski and J. E. McGrath, *J. Membr. Sci.*, 2002, **197**, 231–242.

34 R. K. Singh, K. Kunimatsu, K. Miyatake and T. Tsuneda, *Macromolecules*, 2016, **49**, 6621–6629.

35 C. K. Shin, G. Maier and G. G. Scherer, *J. Membr. Sci.*, 2004, **245**, 163–173.

36 B. Hird and A. Eisenberg, *Macromolecules*, 1992, **25**, 6466–6474.

37 A. Miranda, K. Sarang, B. Gendensuren, E.-S. Oh, J. Lutkenhaus and R. Verduzco, *Mol. Syst. Des. Eng.*, 2020, **5**, 709–724.

38 S. Chauque, F. Y. Oliva, O. R. Cámara and R. M. Torresi, *J. Solid State Electrochem.*, 2018, **22**, 3589–3596.

39 J. Pang, H. Zhang, X. Li, D. Ren and Z. Jiang, *Macromol. Rapid Commun.*, 2007, **28**, 2332–2338.

40 R. M. Gnanamuthu and C. W. Lee, *Mater. Chem. Phys.*, 2011, **130**, 831–834.

41 Q.-C. Zhuang, X.-Y. Qiu, S.-D. Xu, Y.-H. Qiang and S.-G. Sun, *Lithium Ion Batter. – New Dev.*, DOI: 10.5772/26749.

42 S.-D. Xu, Q.-C. Zhuang, L.-L. Tian, Y.-P. Qin, L. Fang and S.-G. Sun, *J. Phys. Chem. C*, 2011, **115**, 9210–9219.

43 P. Liu, W. Zhang, X. Liu, Y. Zhang and F. Wu, *IOP Conf. Ser.: Mater. Sci. Eng.*, 2018, **452**, 032088.

44 D.-W. Jung, J.-H. Jeong and E.-S. Oh, *J. Alloys Compd.*, 2017, **690**, 42–50.

45 S. Park, T. Kim and S. M. Oh, *Electrochem. Solid-State Lett.*, 2007, **10**, A142–A145.

46 J. S. Kim, W. Choi, K. Y. Cho, D. Byun, J. Lim and J. K. Lee, *J. Power Sources*, 2013, **244**, 521–526.